Human Gut Commensal Membrane Vesicles Modulate Inflammation by Generating M2-like Macrophages and Myeloid-Derived Suppressor Cells

Esin Alpdundar Bulut,* Banu Bayyurt Kocabas,† Volkan Yazar,† Gamze Aykut,† Ulku Guler,‡ Bekir Salih,‡ Naz Surucu Yilmaz,* Ihsan Cihan Ayanoglu,* Muammer Merve Polat,§ Kamil Can Akcali,¶ Ihsan Gursel,† and Mayda Gursel*

Immunomodulatory commensal bacteria modify host immunity through delivery of regulatory microbial-derived products to host cells. Extracellular membrane vesicles (MVs) secreted from symbiont commensals represent one such transport mechanism. How MVs exert their anti-inflammatory effects or whether their tolerance-inducing potential can be used for therapeutic purposes remains poorly defined. In this study, we show that MVs isolated from the human lactic acid commensal bacteria *Pediococcus pentosaceus* suppressed Ag-specific humoral and cellular responses. MV treatment of bone marrow–derived macrophages and bone marrow progenitors promoted M2-like macrophage polarization and myeloid-derived suppressor cell differentiation, respectively, most likely in a TLR2-dependent manner. Consistent with their immunomodulatory activity, MV-differentiated cells upregulated expression of IL-10, arginase-1, and PD-L1 and suppressed the proliferation of activated T cells. MVs' anti-inflammatory effects were further tested in acute inflammation models in mice. In carbon tetrachloride–induced fibrosis and zymosan-induced peritonitis models, MVs ameliorated inflammation. In the dextran sodium sulfate–induced acute colitis model, systemic treatment with MVs prevented colon shortening and loss of crypt architecture. In an excisional wound healing model, i.p. MV administration accelerated wound closure through recruitment of PD-L1–expressing myeloid cells to the wound site. Collectively, these results indicate that *P. pentosaceus*–derived MVs hold promise as therapeutic agents in management/treatment of inflammatory conditions. ***The Journal of Immunology*****, 2020, 205: 2707–2718.**

The mammalian gastrointestinal tract harbors hundreds of species of commensal bacteria, which collectively modulate host immunity through a variety of stimulatory or regulatory microbial-derived ligands (1–3). In this context, microbiota members like segmented filamentous bacteria and *Bifidobacterium adolescentis* elicit TH17 cell development (4–6), whereas others, including *Bacteroides fragilis* and certain Clostridia strains support $FOXP3^+$ regulatory T cell (Treg) differentiation and IL-10 production (7–9). Perturbation in immune system–microbiota cross-talk has been correlated with pathogenesis and/or progression of a broad spectrum of diseases, including inflammatory bowel disease, multiple sclerosis, and rheumatoid arthritis (1, 10). Using the immunomodulatory therapeutic potential of gut microbiota or microbiota-associated molecules holds great promise in management/treatment of inflammatory/autoimmune diseases.

One important mechanism by which bacteria manipulate the host immune response is through the secretion of extracellular membrane vesicles (MVs) (11–13). Existence of these vesicles produced by pathogenic Gram-negative bacteria have been shown decades ago (14, 15), whereas the process of MV secretion from Gram-positive bacteria is a more recently discovered phenomenon (16, 17). MVs enable the parent bacteria to deliver much of its biological material, including proteins, DNA, RNA, LPS, peptidoglycan (PGN), and enzymes, in a protective, nonreplicative membranous sphere (11, 17). Considering that MVs represent natural carrier systems for pattern recognition receptor agonists and proteins with antigenic potential, extracellular vesicles from numerous bacteria have been investigated as vaccines or vaccine adjuvant candidates (18–22). To date, bacterial MV–based therapeutics mostly focused on their immunostimulatory potential (18).

*Department of Biological Sciences, Middle East Technical University, Ankara 06800, Turkey; †Therapeutic Oligodeoxynucleotide Research Laboratory, Department of Molecular Biology and Genetics, Ihsan Dogramaci Bilkent University, Ankara 06800, Turkey; ‡Department of Chemistry, Hacettepe University, Ankara 06800, Turkey; §Department of Medical Genetics, Faculty of Medicine, Yuksek Ihtisas University, Ankara 06520, Turkey; and ¶Department of Biophysics, Faculty of Medicine, Ankara University, Ankara 06100, Turkey

ORCIDs: 0000-0001-7506-3717 (B.B.K.); 0000-0003-3861-0181 (V.Y.); 0000-0003-2184-8628 (G.A.); 0000-0002-8542-6531 (B.S.); 0000-0003-4300-1401 (I.C.A.); 0000-0002-6914-485X (M.M.P.); 0000-0003-0044-9054 (M.G.).

Received for publication June 22, 2020. Accepted for publication September 9, 2020.

This work was supported by Scientific and Technological Research Council of Turkey Grant 113S305.

M.G., I.G., and E.A.B. designed the study, and M.G. and E.A.B. analyzed the data and wrote the manuscript. E.A.B. performed all experiments and received assistance from B.B.K., N.S.Y., G.A., and I.C.A. I.C.A. carried out statistical analyses. K.C.A. supervised and M.M.P. performed the liver fibrosis experiments. B.S. supervised and U.G. performed liquid chromatography–tandem mass spectrometry analyses and protein search on membrane vesicles. Bioinformatic analysis of proteomics data was carried out by V.Y.

Address correspondence and reprint requests to Prof. Mayda Gursel, Department of Biological Sciences, Middle East Technical University, 06800 Ankara, Turkey. E-mail address: mgursel@metu.edu.tr

The online version of this article contains supplemental material.

Abbreviations used in this article: AP, alkaline phosphatase; AFM, atomic force microscopy; BMDM, bone marrow–derived macrophage; c-di-GMP, bis-(3′-5′)-cyclic dimeric GMP; 3D, three-dimensional; DSS, dextran sulfate sodium; FMD, foot and mouth disease; FMDV, FMD vaccine; G-MDSC, granulocytic MDSC; GO, Gene Ontology; LAB, lactic acid bacteria; MDSC, myeloid-derived suppressor–like cell; M-MDSC, monocytic subset of MDSC; MRS, de Man, Rogosa, and Sharpe; MS/MS, tandem mass spectrometry; MV, membrane vesicle; MV1, *P. pentosaceus* MV; MV2, *L. salivarious* MV; Nos, NO synthase; PD-L1, programmed cell death ligand 1; PEC, peritoneal exudate cell; PGN, peptidoglycan; PNPP, *p*-nitrophenyl phosphate; SEAP, soluble alkaline phosphatase; αSMA, α-smooth muscle actin; Treg, regulatory T cell.

In contrast, excepting a few studies, our understanding of how bacterial MVs exert immunoregulatory effects and whether we can tap into their tolerance-inducing potential as a new source of anti-inflammatory agents is still incomplete (7, 13, 23).

Lactic acid bacteria (LAB), such as *Lactobacillus salivarius*, are important constituents of the gut and the genitourinary tract microbiota. LAB contribute to gut homeostasis by producing antimicrobial factors (24) and, depending on the species, suppress gut epithelial cell responses to TLR ligands (25–27). Among the large number of LAB species, *Pediococcus pentosaceus* possess potent anti-inflammatory properties and can alleviate encephalopathy and chronic and acute liver injury (28–31). Therefore, in this study, we aimed to test the immunomodulatory therapeutic activity of MVs isolated from the human lactic acid commensal bacteria *P. pentosaceus*. Our results showed that MVs exerted a protective immunomodulatory response in several in vivo acute inflammation models by generating alternatively activated M2 macrophage–like cells and myeloid-derived suppressor–like cells (MDSCs), but not Tregs. Collectively, data suggest that *P. pentosaceus*–derived MVs can be used as potent anti-inflammatory agents for the treatment of inflammatory diseases.

Materials and Methods

Abs, ELISA kits, and reagents

Abs used for flow cytometry were from BioLegend. The specific Abs purchased and their catalog numbers were as follows: allophycocyanin anti-mouse CD274 (B7-H1, programmed cell death ligand 1 [PD-L1]; 124311), FITC anti-mouse F4/80 (123107), PE anti-mouse F4/80 (123110), PE anti-mouse Ly-6C (128008), FITC anti-mouse Ly-6G (127606), PE/Cy7 anti-mouse Ly-6G (127618), PE anti-mouse/human CD11b (101208), Brilliant Violet 605 anti-mouse CD45 (103155), PE anti-mouse/rat/human Foxp3 (320008), and PE/Cy5 anti-mouse CD25 (102010) and Alexa Fluor 488 anti-mouse CD4 (100423). Neutralizing anti-mouse TLR2 Ab was from InvivoGen (C9A12).

ELISA kits for IL-10, IL-6, and TNF-α were purchased from BioLegend and Mabtech. For IgG ELISA, anti-mouse IgG1, IgG2c, and total IgG were purchased from SouthernBiotech. *p*-Nitrophenyl phosphate (PNPP) substrate was from Thermo Fisher Scientific, and TMB substrate solution was from BioLegend. Recombinant cytokines and growth factors used in the study were recombinant mouse M-CSF (Tonbo Biosciences and BioLegend), recombinant mouse GM-CSF (Tonbo Biosciences), and recombinant mouse IL-6 (Tonbo Biosciences). LPS (from *Escherichia coli* O111:B4) was obtained from Sigma-Aldrich. PGN-SA (isolated from the Gram-positive bacterium *Staphylococcus aureus*; TLR2 agonist activity may depend on other commonly purified molecules such as LTA), flagellin (ultrapure flagellin from *Salmonella typhimurium*), and zymosan (cell wall preparation of *Saccharomyces cerevisiae*) were purchased from InvivoGen. Chicken OVA Ag was obtained from Sigma-Aldrich. OVA MHC class I epitope SIINFEKL peptide was obtained from AnaSpec.

Bacterial strains, culture media, and growth conditions

Human commensal bacterial strains used in this study, *P. pentosaceus*, and *L. salivarius* (isolated from human fecal samples) were from Ankara University culture collection and were a kind gift from Dr. F. Kiran. *E. coli* DH5α strain was from American Type Culture Collection (67877).

The de Man, Rogosa, and Sharpe (MRS) medium and MRS agar were purchased from CONDA (Madrid, Spain) and prepared according to the manufacturer's protocol. *P. pentosaceus* and *L. salivarius* were cultured at 37°C overnight in MRS broth medium or MRS agar plates. *E. coli* (DH5α) was grown at 37°C at 150 rpm overnight in Luria broth medium or Luria broth agar.

Isolation of MVs from bacteria

MVs secreted from bacteria were isolated from early steady-state liquid broth cultures. Cell-free supernatants were obtained by centrifugation for 20 min at 6000 rpm, followed by filtration through 0.20-μm filters. Filtered supernatants were centrifuged twice (at 100,000 × *g* for 70 min), and the pellets were resuspended in 30 ml of PBS for centrifugation (70 min at 100,000 × *g*). Finally, pellets were resuspended in PBS (500 μl–1.5 ml), and the MVs were stored at −20°C until further use. Protein content of MVs were determined at 280 nm using a NanoDrop and/or the Micro BCA Protein Assay Kit (Thermo Fisher Scientific).

Average particle size analysis and ζ potential measurements

MVs (1 μg/ml) were diluted 100× with DNase/RNase-free H_2O, and the final volume was adjusted to 1 ml in a polystyrene cuvette suitable for dynamic light scattering analysis. For ζ potential measurements, a disposable capillary cell was used (Nano ZS, Malvern, U.K.). All measurements were carried out using the following parameters: medium refractive index, 1.330; medium viscosity, 0.88 mPa/s; dielectric constant, 78.54; and temperature, 25°C. Measurements were in duplicate, and the results were expressed as the average of two measurements ± SD.

Atomic force microscopy

MVs were diluted (100×) in DNase/RNase-free H_2O prior to deposition onto silicon wafers (5 μl of vesicle per wafer). Samples were air dried for 30 min at room temperature. Noncontact mode images were taken using a PSIA XE-100E model atomic force microscopy (AFM). Multi75Al model tips were from Budget Sensors. Tips' resonance frequency and force constant were 75 kHz and 3 N/m, respectively. Scan rate was kept at 0.73–0.79 Hz. Images were analyzed using XEI 1.6 software.

Cells and culture conditions

OVA-expressing E.G7–EL4 cells (CRL-2113; ATCC) were cultured in RPMI 1640 medium supplemented with 10% FBS and 1 mg/ml neomycin.

HEK-BLUE hTLR2 cells carrying a soluble alkaline phosphatase (SEAP) reporter construct were purchased from InvivoGen (San Diego, CA). Cells were grown in DMEM supplemented with 10% FCS, 2 mM L-glutamine, and 100 μg/ml Normocin in the presence of selection antibiotic and passaged per the manufacturer's recommendation.

For bone marrow–derived macrophage (BMDM) generation, C57BL/6 or BALB/c mice bone marrow progenitor cells were plated in 10-cm petri dishes (1×10^6 cells/ml) or 48-well plates (600,000 cells/ml) and incubated in the presence of 20 ng/ml M-CSF for 6 d. On day 3, fresh 20 ng/ml M-CSF–containing medium was added to the petri dishes (2 ml) or plates (200 μl). Six days after the initiation of culture, cells were stimulated with MVs and/or other ligands.

Differentiation of bone marrow cells by MVs

Bone marrow progenitor cells were incubated with 10 μg/ml MVs in 20% FBS supplemented RPMI 1640 medium. Additional MV-containing media were introduced to cultures on day 3. After 6 d, cells were collected to assess the phenotype of differentiated cells by staining for specific cell-surface markers and imaging the shape of cellular nuclei. NucBlue Live Cell Stain (Molecular Probes) was used to stain nuclei (10 μl/well) by incubation for 15–30 min at room temperature. Cells were visualized using EVOS FLoid cell imaging system (Thermo Fisher Scientific).

In vitro stimulation of cells with MVs

Immunomodulatory effects of MVs were determined in stimulation assays. Mouse splenocytes (400,000 cells per well), peritoneal exudate cells (PECs; 100,000 cells per well), or BMDMs (200,000 cells per well) were stimulated in a total volume of 200 μl in 96-well, flat-bottom plates with three different concentration of MVs (0.2, 1, and 5 μg/ml). PGN (5 μg/ml), zymosan (10 μg/ml), or LPS (1–10 μg/ml) was used as positive controls in stimulations. Cells were incubated at 37°C for 24 h, supernatants were collected, and cytokine levels in culture supernatants were determined with cytokine ELISA. In some experiments, cells were collected from plates and were either fixed with 4% paraformaldehyde and stained or stained without fixation on ice with specific surface markers, followed by flow cytometric analysis.

TaqMan gene expression assay

TaqMan gene expression assay was used to detect two macrophage markers: Arg-1 (arginase; assay identifier: Mm00475988_m1) and NO synthase (Nos) 2 (assay identifier: Mm00440502_m1) (Applied Biosystems). 18S rRNA with reporter VIC/MGB was used as endogenous control, and TaqMan Universal Master Mix II was used as the master mixture.

For RT-PCR, Bio-Rad CFX Connect Real-time system was used. Expression levels were determined by normalization to 18S rRNA.

Flow cytometry analysis

Cells were collected to Eppendorf tubes and centrifuged at 300 × *g* for 5 min. Supernatants were collected for ELISA, and cell pellets were fixed

in 4% paraformaldehyde fixation medium A (Thermo Fisher Scientific) at room temperature for 15 min. After fixation, cells were washed twice in FACS buffer (1% BSA and 0.1% NaN_3 sodium azide in PBS) and stored at 4°C for surface marker staining up to a week. Fixed cells were centrifuged at 300 × *g* for 5 min and resuspended in 100 μl FACS buffer containing 1 μg/ml of fluorochrome-conjugated Abs. Cells were incubated for 30 min in dark at room temperature. After the incubation, 1 ml FACS buffer was added to the cells and centrifuged. Cells were washed with FACS buffer for the last time and resuspended in 200 μl PBS and analyzed on a BD Accuri C6 flow cytometer or NovoCyte flow cytometry (ACEA Biosciences).

In vivo experiments

All animal studies were conducted with prior approval of the Animal Ethics Committee of Bilkent University.

Immunization with foot and mouth disease vaccine in the absence or presence of MVs

Foot and mouth disease (FMD) vaccine was prepared and provided by the FMD Institute (Ankara, Turkey). Six- to eight-week-old female BALB/c mice (five per group) were immunized twice (i.p., days 0 and 17) using the FMD vaccine (FMDV) O/TUR/07 monovalent vaccine (3 μg/mouse) alone or its combination with 10 μg/mouse of 1) *E. coli* MVs, 2) *P. pentosaceus* MVs (MV1), or 3) *L. salivarious* MVs (MV2). FMDV-specific IgG1, IgG2a, and total IgG levels were detected from sera by ELISA 2 wk after each injection. For this, Immulon 1B plates (Thermo Labsystems) were coated with rabbit anti–Ser-O Ab (1:2000 diluted, 50 μl/well) in PBS and incubated overnight at 4°C. As the source of Ag, 1/20 diluted supernatants of FMDV-infected Baby Hamster Kidney (BHK) cells (50 μl/well in blocking buffer) were added and incubated for 2 h at room temperature. Following washing, 80× diluted mouse sera were introduced to the first row of wells and serially diluted 2-fold in PBS containing 1:500 diluted rabbit serum. Plates were incubated overnight at 4°C and washed as before. Goat anti-mouse IgG1/alkaline phosphatase (AP), IgG2a/AP, or IgG total/AP (SouthernBiotech) were 1:3000 diluted in PBS–FBS (5%) (50 μl/well). Following incubation and a final wash, PNPP substrate was added, and color development was recorded at OD 405 nm using a microplate reader (Thermo Fisher Scientific).

To quantitate the number of FMD-specific memory B cells generated in vaccinated mice, ELISpot assay was performed. Four months after the booster injection, mice were sacrificed, and spleens were removed. Single-cell suspensions were prepared, and cell numbers were adjusted to be 10×10^6 cells/ml. All samples were stimulated in six-well plates (10×10^6 cells in 4 ml complete RPMI 1640 supplemented with 10% FBS) for 6 d with a combination of LPS (2 μg/ml) and CpG oligodeoxynucleotide (0.5 μg/ml) to allow for memory B cell expansion and differentiation into Ab-secreting plasma cells. Following washing, cells (1×10^6/200 μl) were plated on rabbit anti–Ser-O Ab/FMDV-infected BHK cell lysate–coated plates and serially diluted 4-fold. After overnight incubation, plates were washed, followed by 50 μl/well goat anti-mouse IgG1/AP or IgG2a/AP (SouthernBiotech) addition (1:3000 diluted in T cell buffer). Plates were washed for the final time and were developed using 70 μl of BCIP-low melting agarose substrate solution (32). The next day, spots were counted using a dissecting microscope.

Immunization of mice with OVA model Ag

Six- to eight-week-old C57BL/6 mice were immunized with OVA model Ag (7.5 μg/mouse) in the absence or presence of MVs (10 μg/mouse) i.p. on days 0 and 14. Primary and secondary bleeding were done on days 15 and 33, respectively. Sera were collected from tail vein blood as before. Immunized mice were challenged s.c. with 4×10^6 E.G7–OVA cells in their right dorsal flanks. Tumor development was measured daily by a caliper and calculated as (length) × (width) × (height) and recorded as cubic millimeters. To assess OVA-specific Ab response, Immulon 1B microtiter plates were coated with 7.5 μg/ml (50 μl/well) OVA, and plates were blocked with 200 μl blocking buffer. The 16× diluted sera were added to the first row of the plate and 4-fold serially diluted eight times. Plates were incubated overnight at 4°C and washed. Following the washing step, AP-conjugated anti-Ig Abs (1000× diluted; total IgG, IgG1, and IgG2c) were added and incubated for 3 h at room temperature. Finally, plates were washed and PNPP substrate was added (50 μl/well). OD values were detected at 405 nm using an ELISA plate reader.

Determination of phenotype of cells generated following i.p. injection of MVs

Eight- to twelve-week-old C57BL/6 mice (five mice per group) were i.p. injected with MVs and PBS as control on days −4 and −1. On day 0, mice were sacrificed by cervical dislocation. PECs and spleen cells were collected. Both PECs and splenocytes were fixed and stained with various cell-surface markers to determine the phenotype of cells generated in response to MV administration.

Zymosan-induced peritonitis model

Eight- to twelve-week-old male C57BL/6 mice were immunized with MVs (10 μg/mouse) and saline on days −3 and −1. On day 0, zymosan (100 μg/mouse) was administered to mice to induce peritonitis. Six hours later, mice were sacrificed, and PECs were collected by injecting 10 ml PBS to peritoneal cavity and collecting resident cells. Collected cells were fixed and surface stained for cell subset analysis.

Dextran sulfate sodium–induced acute colitis model

Eight-week-old C57BL/6 mice were administered 3% dextran sulfate sodium (DSS; 36,000–50,000 m.w., colitis grade) (MP Biologicals) in drinking water for 4 d. MVs (10 μg/mouse) were injected i.p. on days −3 and 0 (pretreatment group) or on days 0 and +3 (posttreatment group). Development of colitis was followed by measuring body weight and examination of blood in stools on a daily basis. After 4 d, drinking water without DSS was provided for an additional 3 d to allow colon epithelial cell recovery. On day 7, colons lengths were measured using a caliper. "Swiss-rolled" colons were placed in 10% buffered formalin solution for further histological analysis.

Wound healing in excisional wound model

Eight- to twelve-week-old BALB/c mice were used for wound healing experiments. Briefly, excisional wounds were introduced using a 6-mm biopsy punch, followed by stabilization with silicone ring splints. MVs (10 μg/mouse) were administered either topically on the wound or by i.p. injections every other day. Wound measurements were conducted for 1 wk, mice were sacrificed, and wound area was removed for histological and flow cytometric cell infiltration analysis. Histological scoring of inflammatory cell infiltration (polymorphonuclear and mononuclear) in H&E-stained sections were given scores as 1, discrete (presence of few inflammatory cells); 2, moderate (many inflammatory cells); and 3, severe (exaggerated inflammatory cellularity) (33). All evaluations were conducted in a blinded fashion.

Proteomics study and mass spectrometry

Fifty micrograms of MV protein sample was reduced with DTT (5 mM) and alkylated using 50 mM iodoacetamide at room temperature for 1 h in dark. Additional DTT was supplemented to achieve the final concentration of 10 mM. Proteins were precipitated using methanol/chloroform precipitation and dissolved in 8 M urea and 50 mM Tris buffer (pH 8.5). The urea concentration was then diluted to 1 M with 50 mM Tris buffer (pH 8.5). Trypsin was dissolved in 50 mM Tris buffer (pH 8.5) and then added to the protein solution at a ratio of 1:100 (w/w, trypsin/protein). As such, treated samples were incubated overnight, followed by trifluoroacetic acid addition (0.5% v/v) to stop the enzymatic digestion. The samples were cleaned using Sep-Pak (Waters) according to the manufacturer's protocol. Samples were dried using Speed-Vac centrifugal evaporator and then dissolved in MilliQ water (18.2 MΩ.cm) to a final protein concentration of 0.5 μg/μl. Liquid chromatography–tandem mass spectrometry (MS/MS) analyses were performed by trapped ion mobility spectrometry–time-of-flight mass spectrometer equipped with a CaptiveSpray nanoBooster source (Bruker Daltonics, Bremen, Germany) coupled to an Ultimate 3000 RSLCnano system (Dionex, Thermo Fisher Scientific).

Proteomics analysis

The raw data from mass spectrometry were analyzed through the ProteinScape version 4.0 for peptide and protein identification. The Mascot search engine searched MS/MS data against the SwissProt database (bacteria). Following the initial proteomics analysis, "Retrieve/ID Mapping" tool by Uniprot was used for a final list of 103 identifiers to retrieve corresponding UniProtKB proteins and, ultimately, to obtain relevant Gene Ontology (GO) terms separately for each close species used to annotate Mascot input during the annotation step. A total of 275 hits were percentage scaled for the cumulative frequency of each GO term observed. The R function "plotrix" in the Plotrix package was used to create the three-dimensional (3D) pie chart with the following parameters: explode = 0.1 and $\theta = \pi/4$. Secretome analysis was performed on the same dataset, with 103 identifiers using the SecretomeP 2.0 software. An SecP score of 0.5 for possible secretion was set as threshold, as suggested by Bendtsen et al. (34).

Statistical analysis

Statistical analyses were performed with GraphPad Prism 6 and R (v3.3.3). For statistical comparison of two means, normality was tested by Shapiro–Wilk test. If samples fit to normal distribution, means were statistically compared by using unpaired *t* test with Welch correction. Otherwise, means were compared by Mann–Whitney *U* test. For the comparison of more than two means, assumptions of ANOVA (normality and equality of variances) were checked by Shapiro–Wilk test and Brown–Forsythe test. If assumptions were found to be valid, means were statistically compared by using one-way ANOVA, followed by either Dunn or Holm–Sidak multiple comparison tests. If at least one of the assumptions was found to be violated, means were statistically compared by using Kruskal–Wallis test, followed by Dunn multiple comparison test, and $p < 0.05$ was considered significant. Statistical tests used in each figure are specified in the figure legends together with exact *p* values.

Results

P. pentosaceus *MVs suppress inflammation-induced liver fibrosis and vaccination-induced humoral and cellular immunity*

Whether gut-resident LAB secrete MVs and how such MVs impact the immune system is currently unknown. To address these, we first purified MVs secreted from two human gut commensal bacteria isolates (*P. pentosaceus* and *L. salivarius*) and from *E. coli*. Images of purified MVs were captured using AFM. Vesicles appeared to be spherical, consistent with closed membrane morphology (Fig. 1A). Dynamic light scattering measurements showed that *E. coli* MVs had an average size of ∼200 nm, whereas commensal-derived MVs were much larger (∼325–425 nm; Fig. 1B). As expected, MVs had high negative ζ potentials that ranged between −35 and −45 mV (35) (Fig. 1C). To confirm that MVs could be reproducibly purified with no major alterations in their content, three separate *P. pentosaceus* cultures were initiated, followed by MV purification. The protein content of these batches was compared using SDS-PAGE (Supplemental Fig. 1). Different batches of MVs contained identical proteins of similar concentrations, confirming the consistency of MV production and isolation procedure. These vesicles were also subjected to proteomic analysis. Species-specific functional data for *P. pentosaceus* were retrieved from Uniprot database for GO term analysis and the functional enrichment. The resulting MS/MS spectra of peptides identified in the *P. pentosaceus* MVs were searched against the genome of the bacterium itself, along with those of the evolutionarily closest relatives identified automatically by the Mascot algorithm. A total of 103 proteins were identified in the MVs (Supplemental Table I). Of these, a substantial proportion was identified as of intracellular and/or cytoplasmic origin (Fig. 1D). Contrary to Gram-negative MVs in which membrane-associated proteins are abundant, Gram-positive MV constituents predominantly arise from cytosolic/cytoplasmic compartments (36). Similarly, a secretome analysis revealed that out of the 103 proteins identified in *P. pentosaceus* MVs, a total of 19 proteins were predicted to be secreted, which complies with the range estimated for Gram-positive bacteria (34).

To determine whether commensal LAB MVs could modify inflammatory responses, the effect of systemic MV administration was tested in an Ag-independent chronic inflammation model. For this, liver fibrosis was induced in C57BL/6 mice by i.p. injection of

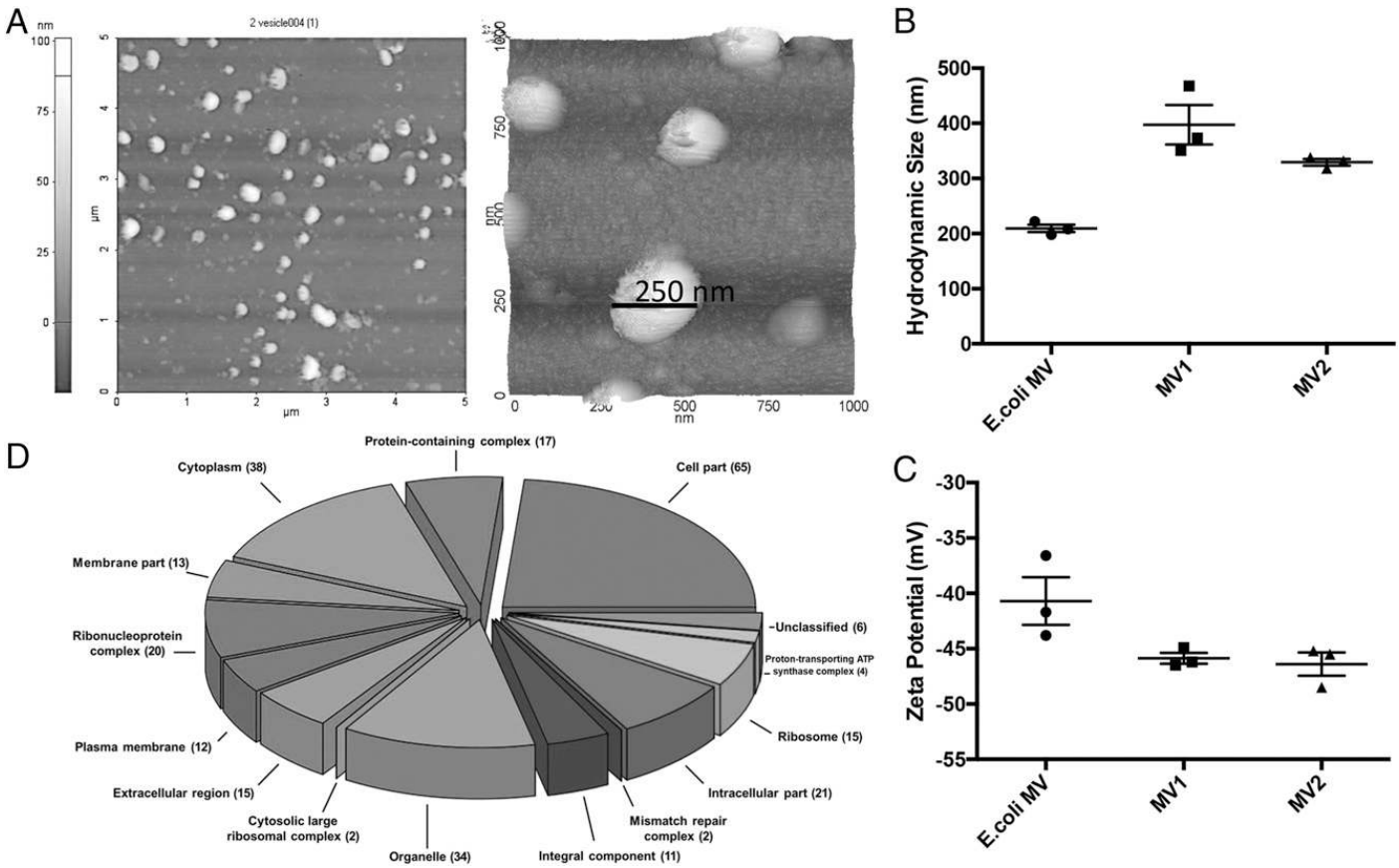

FIGURE 1. Characterization of *P. pentosaceus* MVs. (**A**) AFM images of *L. salivarius* MVs. Topographic image of a 5 × 5 (μm) region containing numerous MVs (left) and 3D scan of MVs (1 × 1 μm region, right) are shown. The AFM results are representative of at least two independent samples. Hydrodynamic size (**B**) and ζ potential (**C**) of *E. coli* MV, MV1 (*P. pentosaceus*), and MV2 (*L. salivarius*) were measured by dynamic light scattering. Measurements from three independent samples ± SEM are shown. (**D**) Pie chart depicting the functional classification of 103 proteins identified in *P. pentosaceus* MVs. Uniprot Retrieve/ID Mapping tool was used to obtain the GO term hits. Hits were percentage scaled for the cumulative frequency of each GO term observed. The R function plotrix in the Plotrix package was used to create the 3D pie chart with the following parameters: explode = 0.1 and θ = π/4. Proteomics data show that the constituents of *P. pentosaceus* MVs predominantly arise from cytosolic/cytoplasmic compartments.

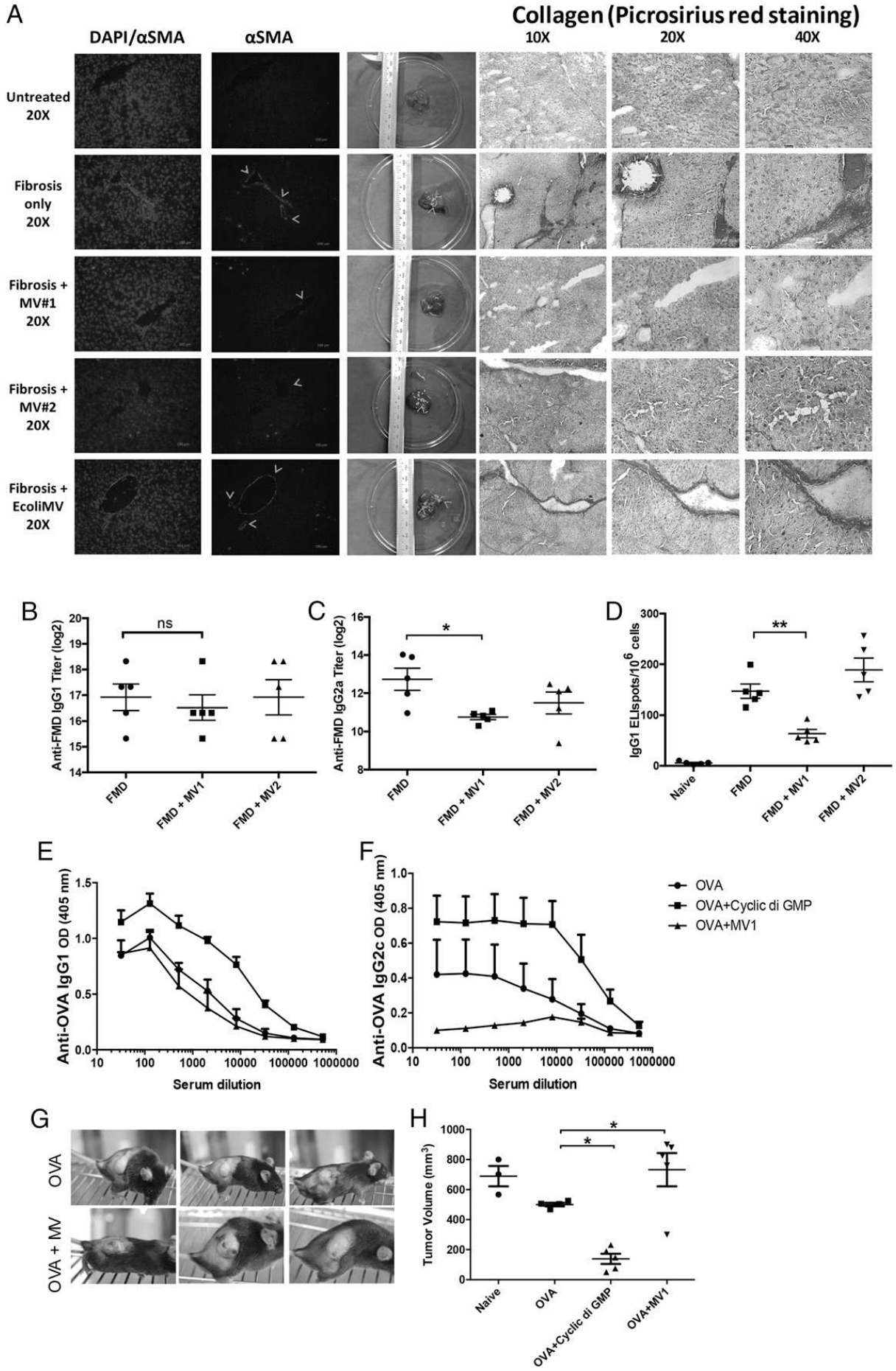

FIGURE 2. *P. pentosaceus* MVs suppress Ag-independent and Ag-dependent immune responses in mice. (**A**) Liver fibrosis-induced mice were either untreated or treated with three i.p injections (2 d apart) of one of the following MVs isolated from *P. pentosaceus* (MV1), *L. salivarius* (MV2), or *E. coli*. Severity of fibrosis was evaluated based on expression/accumulation αSMA and collagen by immunofluorescence and Picrosirius red staining. Fibrotic lesions are shown by arrowheads). (**B** and **C**) FMDV-specific IgG responses of mice immunized with FMD Ag (3 μg/mouse) or its combination with MVs (n = 5). The p values were determined using one-way ANOVA and Dunnett multiple comparison test. *p = 0.0232. IgG1 *(Figure legend continues)*

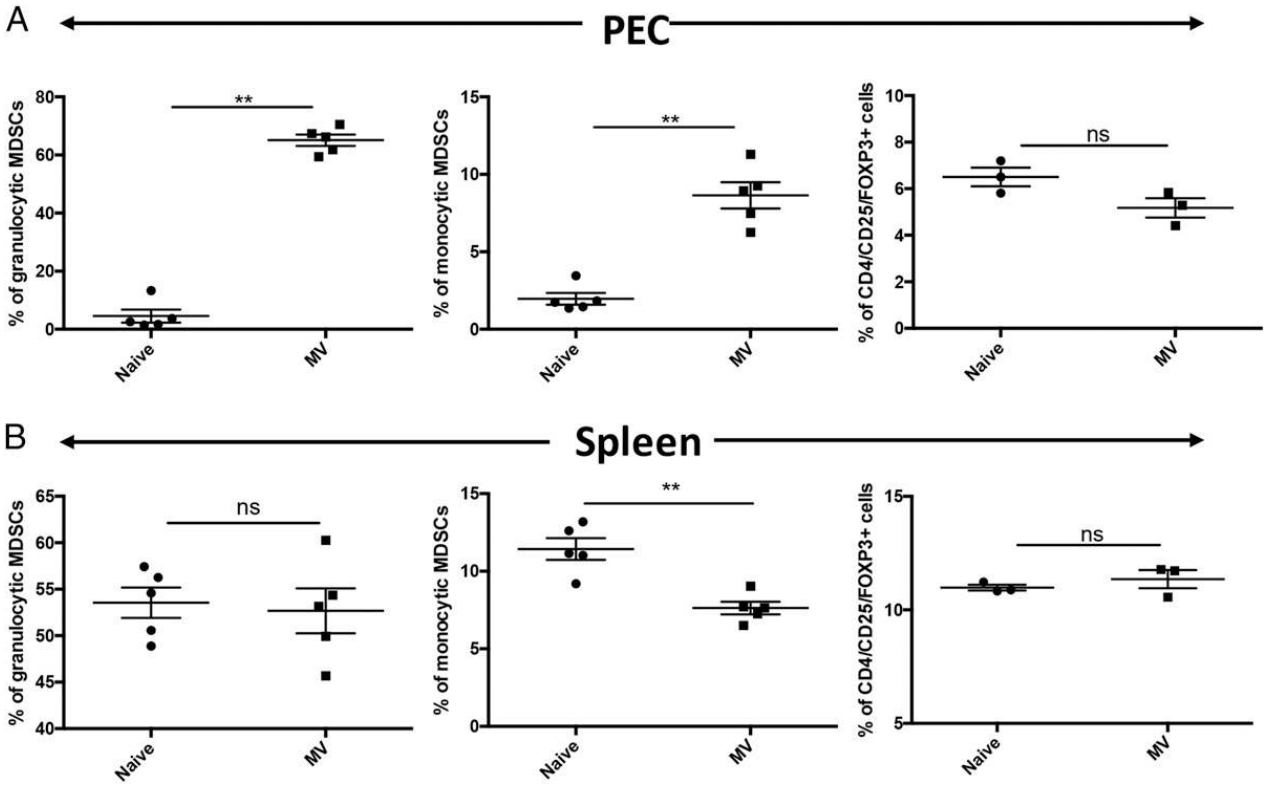

FIGURE 3. An i.p. injection of *P. pentosaceus* MVs promotes MDSC accumulation in the peritoneal cavity. C57BL/6 mice were i.p. injected with MVs (10 μg/mouse) or control saline on days −4 and −1. Mice were sacrificed on day 0, and PECs (**A**) or spleen cells (**B**) were isolated and analyzed by flow cytometry. Percentages of granulocytic MDSC, monocytic MDSCs, and Tregs in individual mice are shown. Error bars represent ± SEM (n = 3–5). $^{**}p = 0.0079$, tested by two-tailed Mann–Whitney U test.

carbon tetrachloride (CCl4) twice a week for 4 wk. Fibrosis-induced groups were either untreated or treated with three i.p. injections (2 d apart) of one of the following MVs isolated from *E. coli*, *P. pentosaceus* (MV1), or *L. salivarius* (MV2). Effect of MV treatment on the severity of liver fibrosis was evaluated based on expression/accumulation of two different fibrosis indicators, α-smooth muscle actin (αSMA), and collagen by immunofluorescence and Picrosirius red staining, respectively (Fig. 2A). Commensal, but not *E. coli*, MV administration resulted in decreased αSMA expression and collagen accumulation in the liver, suggesting that commensal MVs had a protective effect in this model.

Next, effect of these extracellular vesicles on the development of Ag-specific immune response was tested in a vaccination model. Inactivated FMDV without the adjuvant Montanide ISA 720 was used as the model vaccine. Six- to eight-week-old female BALB/c mice were immunized twice with the FMDV in the absence or presence of MVs. FMD-specific secondary IgG1 and IgG2a responses were evaluated 2 wk after the booster injection. Results showed that *P. pentosaceus* MV–adjuvanted group did not alter Ag-specific IgG1 when compared with the FMDV alone (Fig. 2B). Notably, commensal MV–adjuvanted groups decreased IgG2a titers, which was significantly lower in the case of *P. pentosaceus* MV–administered group ($p = 0.0232$). These results suggest that commensally derived MVs modulate Th1 responses and, hence, abate FMD-specific IgG2a production (Fig. 2C).

To assess how memory B cell responses were affected in MV-adjuvanted groups, splenocytes from vaccinated mice were incubated with LPS plus CpG oligodeoxynucleotide combination for 5 d to enable memory B cell expansion and differentiation into Ab-secreting plasma cells. FMD-specific IgG production was evaluated by ELISpot (Fig. 2D). Results showed that *P. pentosaceus* MV–adjuvanted group caused a significant decrease in the number of memory B cells generated when compared with FMDV (2.3-fold decrease, $p = 0.0016$; Fig. 2D). MVs isolated from *L. salivarius* had no such effect. These results suggested that depending on the bacterial species, commensal bacteria–derived vesicles subsided memory B cell responses. Because *P. pentosaceus* MVs showed a more pronounced immunoregulatory effect, hereafter, only vesicles from this source were used in other experiments.

To confirm that *P. pentosaceus* MVs' inhibitory effect on Th1-dependent IgG2a class switching was not limited to the FMDV alone, tolerogenic effect of MVs was assessed in a second immunization model. Consistent with previous results, in an OVA-vaccination model, *P. Pentosaceus* MVs specifically suppressed OVA-specific IgG2c, but not IgG1, production when compared with OVA alone or OVA adjuvanted with bis-(3′-5′)-cyclic dimeric GMP (c-di-GMP) (Fig. 2E, 2F). To further test whether MVs suppressed cell-mediated immunity, immunized mice were challenged with s.c. injection of OVA-expressing E.G7 tumorigenic thymoma cells. Tumor growth was monitored, and representative tumor images and tumor sizes were obtained 14 d after

spot-forming cells were enumerated by ELISpot (**D**). Statistical significance was tested by one-way ANOVA and Holm–Sidak multiple comparisons test. $^{**}p = 0.0016$. (**E** and **F**) Anti-OVA–specific IgG responses of C57BL/6 mice immunized on days 0 and 14 with OVA (7.5 μg/mouse), OVA + MV (10 μg/mouse), or OVA + c-di-GMP (15 μg/mouse; $n = 5$). Mice were inoculated with OVA-specific E.G7 thymoma cells (4×10^6 cells per mouse) for tumor challenge. Representative images of tumors (**G**) and tumor volumes (**H**) 14 d after inoculation. Statistical significance was tested by one-way ANOVA Holm–Sidak multiple comparisons test. $^{*}p = 0.0110$, OVA versus OVA c-di-GMP; $^{*}p = 0.0494$, OVA versus OVA MV.

challenge are shown in (Fig. 2G, 2H). MV-adjuvanted OVA groups exacerbated tumor formation ($p = 0.0494$), whereas c-di-GMP adjuvantation triggered significant protective antitumor immunity ($p = 0.0110$) when compared with OVA alone. Collectively, these results indicate that *P. pentosaceus* MVs negatively regulate Th1-dominated cellular immune responses.

P. pentosaceus *MVs promote MDSC differentiation and M2 macrophage polarization in vitro and in vivo*

To gain insight into the mechanism of the MV-mediated immune modulation, C57BL/6 mice were i.p. injected with MVs (10 μg/mouse) or saline (naive group) on days −4 and −1. On day 0, mice were sacrificed, and PEC and spleen cells were collected and stained for monocytic subsets of MDSC (M-MDSC)-specific or granulocytic MDSC (G-MDSC)-specific markers (CD11b, Ly-6G, and Ly-6C) or Treg markers (CD4/CD25/Foxp3). A gating strategy to include single cells (FSC-A/FSC-H plot) and CD11b-positive cells (CD11b/FSC-H plot) was used as shown in Supplemental Fig. 2. Granulocytic MDSCs were defined as Ly-6G–positive and Ly-6C–dim cells (Supplemental Fig. 2A, 2B, R3 gate), whereas monocytic MDSCs were gated as Ly-6C–positive and Ly-6G–negative cells (Supplemental Fig. 2A, 2B, R2 gate). MV administration had no effect on percent of G-MDSCs, whereas M-MDSCs levels were slightly decreased in the spleen when compared with naive controls (Fig. 3B). Similarly, MV injection did not alter Treg percentages in spleen or PEC (Fig. 3). In contrast, significant numbers of both granulocytic and monocytic MDSCs accumulated in the peritoneal cavity of MV-administered mice when compared with PBS-treated mice ($p = 0.0079$; Fig. 3A). These results suggest that MVs act specifically on myeloid cells and stimulated both M-MDSC and G-MDSC, but not Treg, development in vivo.

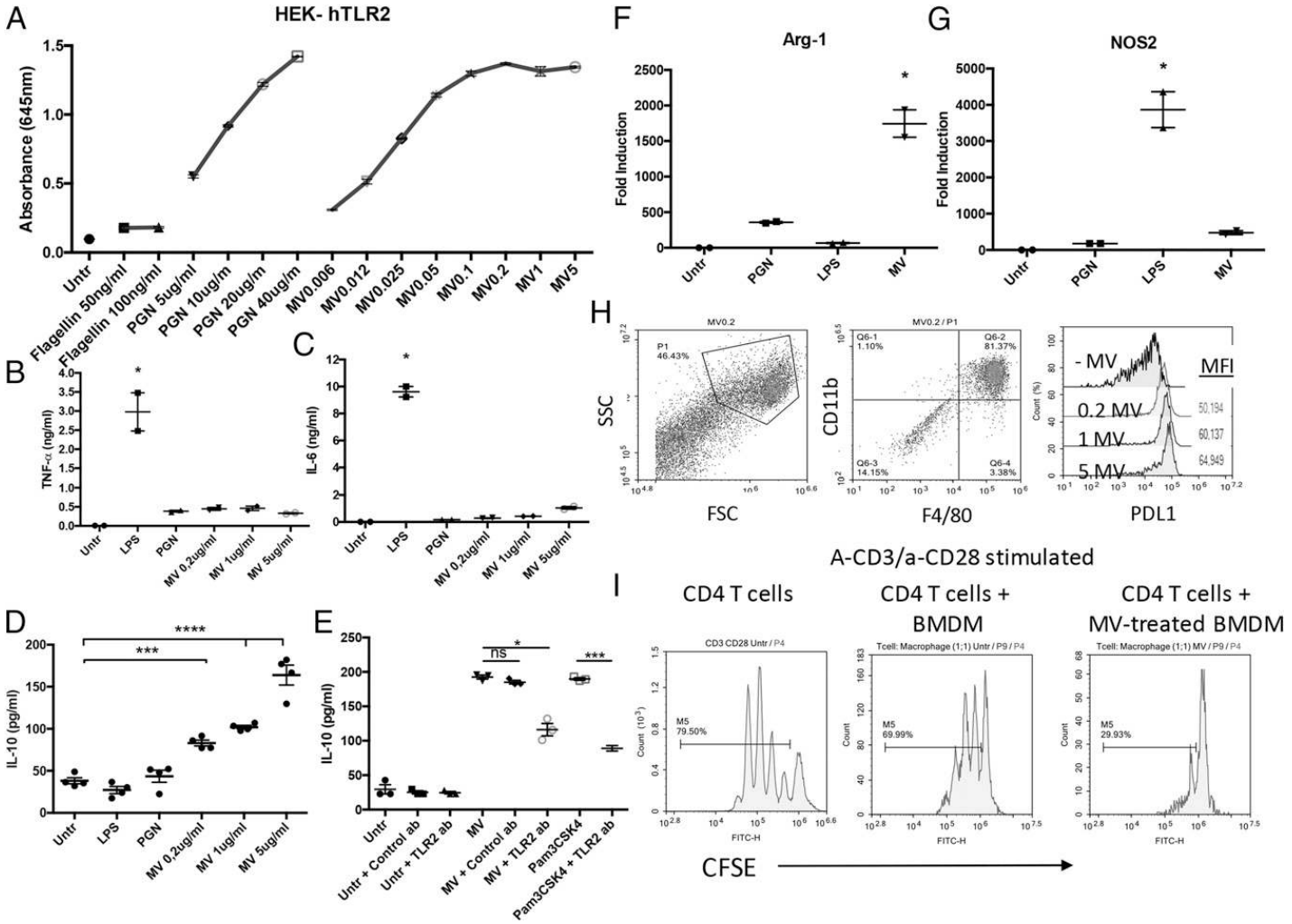

FIGURE 4. *P. pentosaceus* MVs promote MDSC differentiation and M2 macrophage polarization. (**A**) HEK-Blue hTLR2 cells expressing an NF-κB–inducible SEAP reporter gene were stimulated with various doses of MVs, positive control peptidoglycan (PGN), or negative control flagellin for 24 h. Activation-induced SEAP production was assessed in the culture supernatant using QUANTI-Blue. (**B**–**G**) BMDMs were stimulated with the indicated ligands for 24 h. Culture supernatants were assessed by ELISA for levels of TNF-α (B), IL-6 (C), and IL-10 (D) production. The TLR2 dependency of MV- or Pam3CsK4-induced IL-10 production from BMDMs was assessed in the presence of TLR2-neutralizing or isotype control Abs (E). Relative mRNA levels for Arg-1 (F) and Nos2 (G) compared with 18S rRNA expression were assessed using the ΔΔcT-method. (**H**) Histogram depicting PD-L1 expression in MV-treated or -untreated BMDMs. CD11b and F4/80 double-positive cells were gated for PD-L1 expression analysis. (**I**) Representative histograms showing the suppressive effect of MV-treated BMDMs. CFSE-labeled anti-CD28/anti-CD3–stimulated $CD4^+$ T cells were used as such (left panel) or cocultured with BMDMs (middle panel) or MV-treated BMDMs (right panel) for 72 h. Except for the representative flow cytometry plots, individual data points and means ± SEM were reported ($n = 2$–4 independent experiments). All treatments were compared with untreated cells. The following statistical analyses were used for each figure. (B) Kruskal–Wallis test and Dunn multiple comparisons test. *$p = 0.0273$. (C) Kruskal–Wallis test and Dunn multiple comparisons test. *$p = 0.0277$. (D) Ordinary one-way ANOVA and Holm–Sidak multiple comparisons test. ***$p = 0.0003$, ***$p = 0.0001$. (E) Kruskal–Wallis test and Dunn multiple comparisons test. *$p = 0.0225$. Statistical significance between Pam3CSK4 and Pam3CSK4 + TLR2 Ab was tested by unpaired *t* test with Welch correction. ***$p = 0.0003$. (F) Kruskal–Wallis test and Dunn multiple comparisons test. *$p = 0.0429$. (G) Kruskal–Wallis test and Dunn multiple comparisons test. *$p = 0.0395$.

TLR2-mediated signaling has been shown to play an essential role in MDSC induction (37). To determine whether *P. Pentosaceus* MVs harbored TLR2-stimulating agonists, HEK-BLUE hTLR2 reporter cells were stimulated with various doses of MVs, PGN (positive control), or flagellin (negative control). Results showed that MVs dose-dependently stimulated NF-κB–inducible SEAP production in the reporter cells (Fig. 4A). Because TLR2 agonists can promote immunosuppressive M2 macrophage development (38–40), we next investigated the effect of MVs on macrophage polarization. For this, BMDMs were generated from bone marrow progenitors using M-CSF and then stimulated with three different concentration of MVs or with the M1-polarizing ligand LPS or the M2-polarizing ligand PGN. MV-treated macrophages secreted lower levels of TNF-α and IL-6 than LPS-stimulated samples (Fig. 4B, 4C). In contrast, MVs dose-dependently stimulated robust IL-10 secretion from BMDMs (Fig. 4D). IL-10–promoting activity of MVs was significantly reduced when TLR2 was blocked by a neutralizing Ab ($p = 0.0225$; Fig. 4E), suggesting that TLR2-mediated recognition plays an important role in MV-dependent macrophage polarization. To confirm the nature of this polarization, mRNA expression of inducible Nos2 or arginase (Arg-1) was analyzed by RT-PCR as indicators of M1 or M2 polarization, respectively. Consistent with their role in promoting M2 differentiation, MVs strongly upregulated the expression of Arg-1 ($p = 0.0429$; Fig. 4F), but not Nos2 (Fig. 4G). Furthermore, MV treatment strongly upregulated PD-L1 expression on BMDMs (Fig. 4H), implicating that PD-L1/PD-1 interaction might play a critical role in mediating the immunosuppressive function, MV-treated myeloid cells. To confirm that MV-stimulated BMDMs acquire T cell suppressive immunomodulatory activity, CFSE-labeled, TCR-activated CD4+ T cells were cocultured with untreated or MV-treated BMDMs. TcR ligation of CD3 along with CD28 (CD3/CD28) resulted in robust T cell proliferation, as evidenced by CFSE dye dilution (Fig. 4I). Coculture with MV-treated, but not MV-untreated, BMDMs substantially inhibited proliferation in T cells (Fig. 4I).

Collectively, these results indicate that MV treatment of BMDM support M2-like immunosuppressive macrophage polarization. It is likely that such M2-like BMDMs inhibit T cell proliferation through IL-10, arginase-1–mediated depletion of L-arginine, and/or through PD-L1/PD-1 pathway.

Because our in vivo data indicated that MV administration promoted induction of MDSC-like cells (Fig. 3), we next investigated whether MV treatment could directly act on bone marrow progenitors to stimulate MDSC development. Briefly, bone marrow progenitor cells were incubated in the presence of MVs without or with M-CSF for 6 d. M-CSF only–treated progenitors served as the BMDM control and were then differentiated into M1 or M2 macrophages following incubation in the presence of LPS or PGN, respectively. Consistent with previous results, MV-stimulated samples supported the differentiation of IL-10–producing cells from progenitors (Fig. 5A). Importantly, MV activity was direct and did

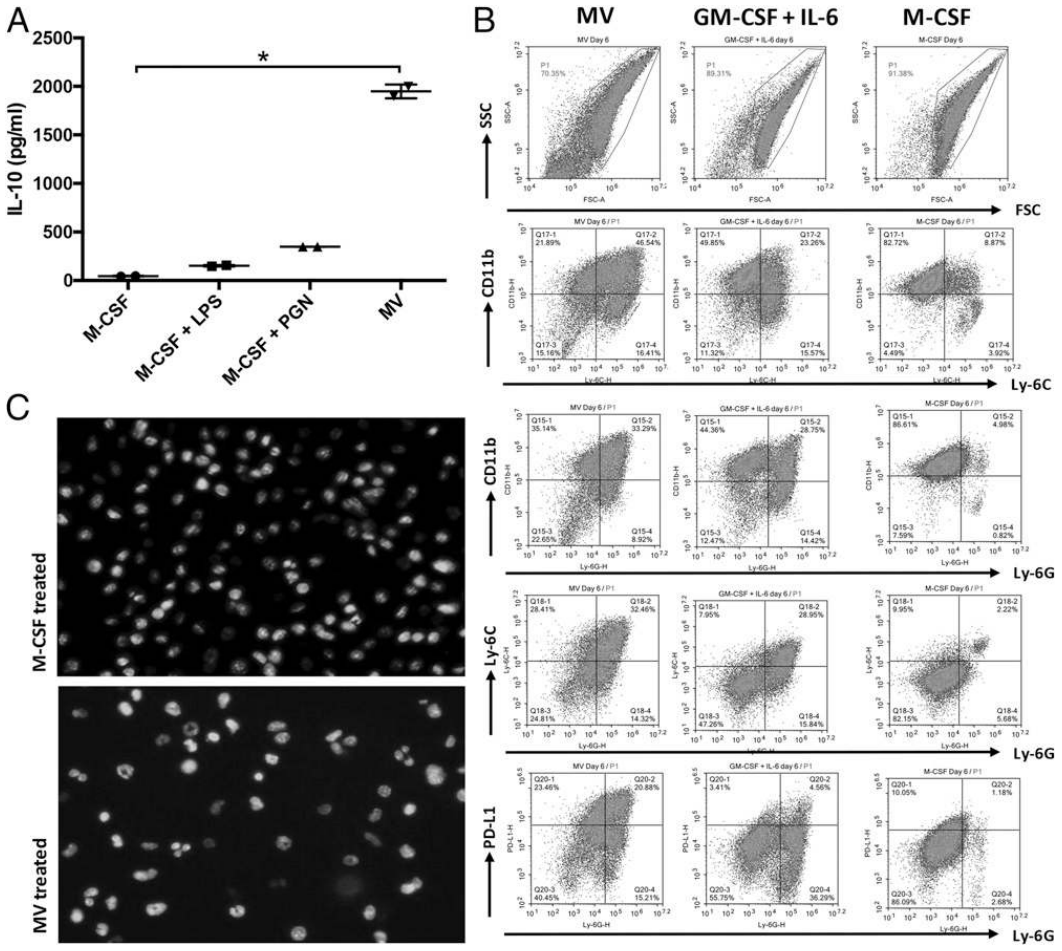

FIGURE 5. MVs program differentiation of bone marrow precursors into MDSC-like cells. Bone marrow precursor cells were incubated in the presence of M-CSF (20 ng/ml), M-CSF (20 ng/ml) + LPS (1 μg/ml), M-CSF (20 ng/ml) + PGN (5 μg/ml), or MVs (10 μg/ml) for 6 d. After the incubation period (**A**) supernatant IL-10 levels were detected by ELISA. Data are representative of two independent experiments. Error bars represent ± SEM. Statistical significance was tested by Kruskal–Wallis and Dunn multiple comparisons test. *$p = 0.0429$. (**B**) Flow cytometric analysis of CD11b, Ly-6C, Ly-6G, and PDL-1 expression in bone marrow precursors treated for 6 d with MVs (left), GM-CSF + IL-6 (to generate MDSCs; middle), or M-CSF (to generate BMDMs; right). (**C**) M-CSF (top)– or MV (bottom)–treated cells were stained with NucBlue Live Cell Stain to analyze nuclear morphology. The images were taken at original magnification ×20 under EVOS FLoid cell imaging station (data are representative of three independent experiments).

not require additional growth factors (i.e., M-CSF). To determine the phenotype of cells differentiating in response to direct MV treatment, bone marrow progenitors were treated with MVs and compared with cells differentiated in the presence of M-CSF or GM-CSF + IL-6 as BMDM and MDSC controls, respectively. All treatments resulted in differentiation of CD11b+-positive cells (Fig. 5B). However, only the MV- or GM-CSF + IL-6, but not the M-CSF, cultures generated Ly-6C/Ly-6G–expressing cells in support of MDSC development. Notably, MV-differentiated samples uniquely expressed high levels of PD-L1 (Fig. 5B). Microscopic examination of the MV-differentiated cells demonstrated a significant phenotypic heterogeneity, which included cells with doughnut-shaped nuclei typical of G-MDSC (Fig. 5C, lower panel). Such ring-shaped nuclei were absent in M-CSF–generated BMDM (Fig. 5C, upper panel). These results demonstrate that MVs program the differentiation of bone marrow precursors into MDSC-like cells.

P. pentosaceus *MV therapy affords protection in experimental models of inflammation and wound healing*

Having established that *P. pentosaceus* MVs induced immunosuppressive cells of myeloid lineage, we next wanted to investigate their therapeutic utility as protective agents in experimental models of inflammation and wound healing.

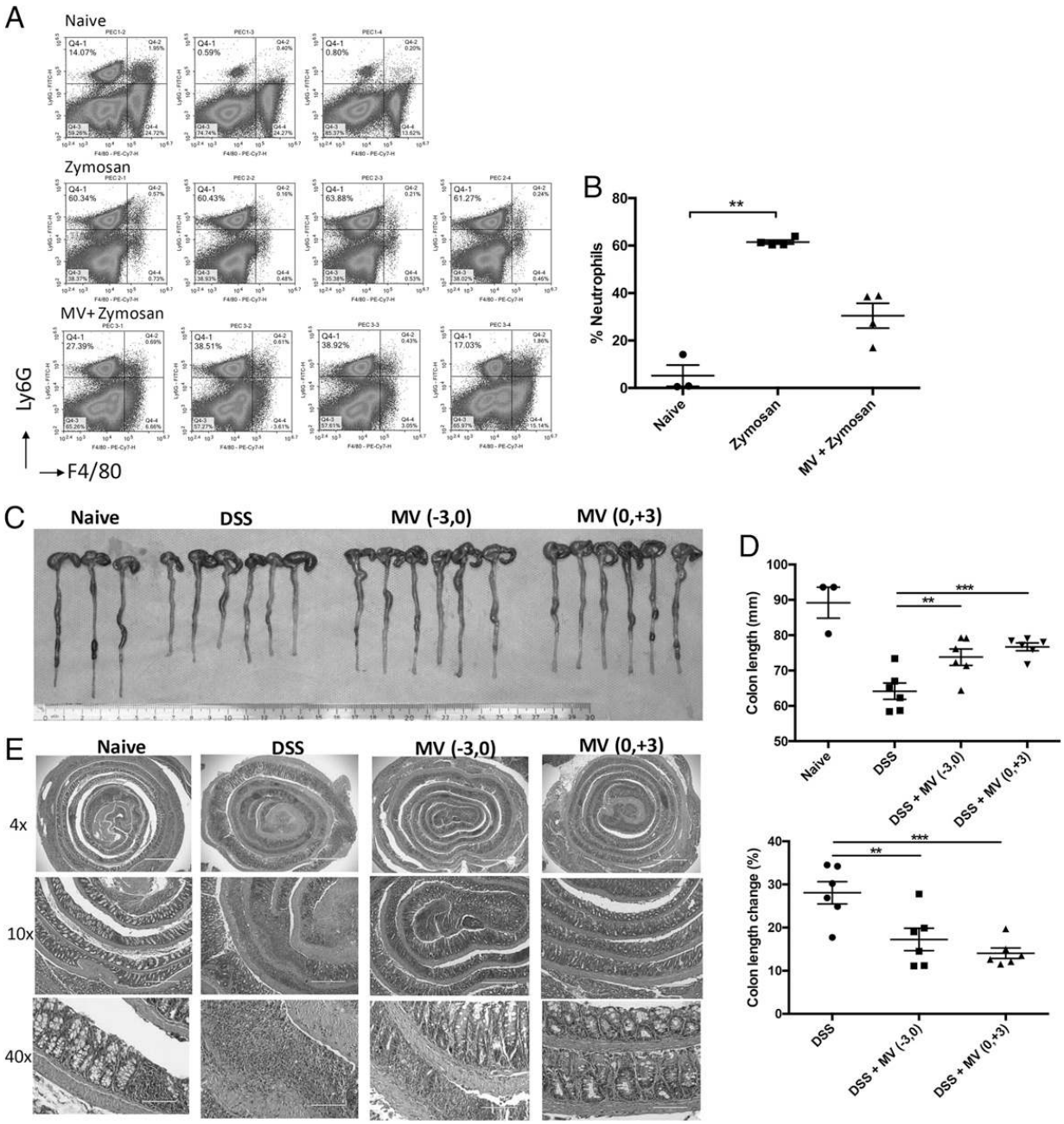

FIGURE 6. Systemic MV administration suppress inflammation in zymosan-induced peritonitis and acute DSS-induced colitis. (**A**) C57BL/6 mice were pretreated with MVs or control saline on days −3 and −1. Zymosan was injected i.p. on day 0. Six hours later, PECs were collected and stained for neutrophil markers and analyzed by flow cytometer. (**B**) Percentage of neutrophils in individual mice. Error bars represent ± SEM ($n = 4$). $^{**}p < 0.0092$, tested by Kruskal–Wallis test and Dunn multiple comparisons test. (**C**–**E**) C57BL/6 mice received 3% DSS in drinking water for 4 d, followed by regular water supplementation for 3 d. MVs (10 μg/mouse) were injected i.p. on days −3 and 0 (pretreatment group) or on days 0 and +3 (posttreatment group). (C) Macroscopic appearance of excised colons in naive (no DSS), DSS-treated, DSS + MV–pretreated, and DSS + MV–posttreated mice 7 d after DSS administration.(D) Colon lengths were measured (top), and percentage change in colon lengths (bottom) are displayed. Error bars represent ± SEM ($n = 5$). Statistical significance was tested by ordinary one-way ANOVA and Holm–Sidak multiple comparisons test. $^{**}p = 0.0038$, $^{***}p = 0.0010$. (C) Representative images of histopathological changes in colon tissue samples examined by H&E staining are displayed (original magnification ×4, original magnification ×10, original magnification ×40).

In a zymosan-induced acute peritonitis model, preadministration of MVs on days −3 and −1 of peritonitis induction resulted in significantly decreased neutrophil accumulation into the peritoneal cavity, consistent with reduced inflammation (Fig. 6A, 6B).

Anti-inflammatory protective effects of MVs were also tested in a DSS-induced colitis model. Mice were supplemented with 3% DSS in drinking water for the first 4 d, followed by plain drinking water without DSS for 3 more d to allow epithelial recovery. Severity of colitis was deduced from colon lengths. Colons of mice in DSS-induced colitis group had significant reduction in length when compared with naive controls (Fig. 6C, 6D), indicating inflammation-associated pathology. In contrast, MV-treated groups had reduced colon shortening, which was statistically not different from the healthy control group. When percent colon length changes were compared, both pre- and posttreatment MV administration protected against DSS-induced colitis ($p = 0.0038$ and $p < 0.0010$ for pre- and posttreatment groups, respectively). Isolated colons were prepared as Swiss rolls and histologically

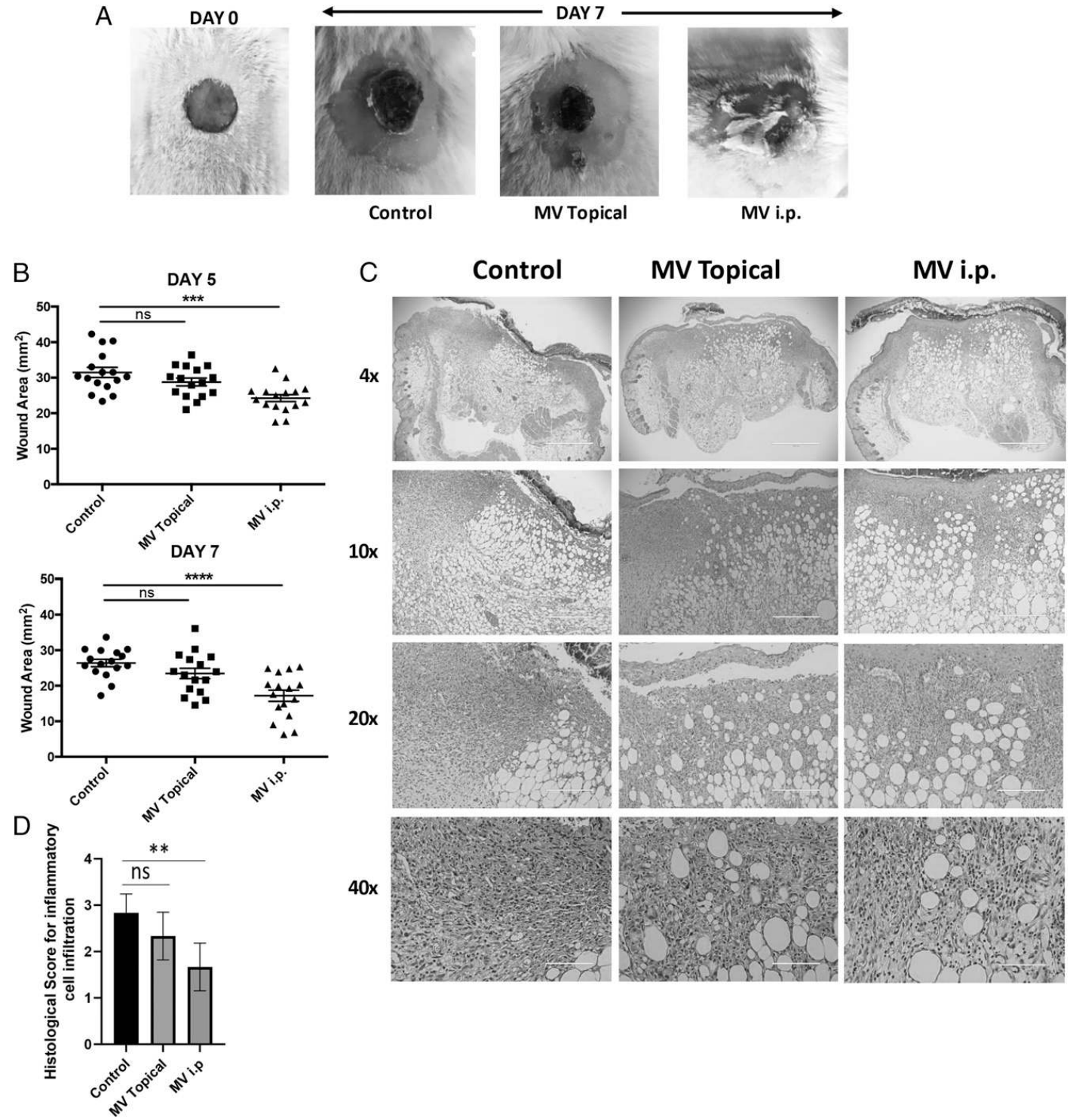

FIGURE 7. MVs accelerate wound healing in an in vivo excisional wound model. Excisional wounds were introduced to dorsal skin of BALB/c mice by a 6-mm biopsy punch. MVs (10 μg/mouse) were administered every second day either i.p. or topically. Length and width of the wound area were measured every second day. (**A**) Representative image of wound area on days 0 and 7. (**B**) Individual wound area measurements on days 5 (top) and 7 (bottom) ($n = 15$, compiled from two independent experiments) ± SEM are shown. Statistical significance was tested by ordinary one-way ANOVA Dunnett multiple comparisons test. ***$p = 0.0002$, ****$p = 0.0001$. (**C**) Representative images of H&E staining of skin tissue isolated from the wound site (original magnification ×4, original magnification ×10, original magnification ×20, and original magnification ×40). (**D**) Histological scoring of inflammatory cell infiltration in wounds. Statistical significance was tested by ordinary one-way ANOVA Dunnett multiple comparisons test. **$p = 0.0015$.

analyzed in H&E-stained, sectioned samples. Fig. 6E shows that colon sections of naive mice display intact colonic crypt organization. In contrast, in DSS-treated mice, crypt architecture was disrupted and accompanied by inflammation and tissue damage. Both pretreatment and posttreatment with MVs ameliorated disease progression, and the crypt architecture was protected in both pre- and posttreatment groups (Fig. 6E).

Because our data also indicated that MVs supported the differentiation of alternatively activated wound healing M2-like macrophages, we hypothesized that MV treatment would prove to be of benefit in a wound healing model. To test this hypothesis, cutaneous excisional wounds were introduced in BALB/c mice. MVs were either directly applied to the wound area topically or were administered through i.p. injection every second day for 6 d after wound excision. Systemic treatment with MVs significantly improved the wound closure, with a wound area smaller than that in untreated controls, as indicated in Fig. 7A and 7B ($p = 0.0002$ and $p = 0.0001$ at days 5 and 7, respectively). Topical administration of MVs had no significant effect on wound healing. Histological analysis of excised wounds showed that i.p MV-treated group had lower levels of inflammatory cell infiltration at the wound site (Fig. 7C, 7D; $p = 0.0015$). In untreated controls, higher levels of inflammatory cell infiltrate and cell debris were observed, indicative of ongoing inflammatory phase, whereas in MV-treated groups, histological findings were consistent with the resolution/remodeling phase of wound healing. To analyze the phenotype of cells responsible for accelerated healing in systemic MV-treated wounds, single-cell suspensions from Liberase-treated wounds were stained for CD11b, Ly-6G, and PD-L1 expression. Results demonstrated that i.p. administration of MVs led to significantly higher numbers of MDSC recruitment to the wound area when compared with the control group ($p = 0.0225$; Supplemental Fig. 3). These results suggest that i.p. administration of MVs accelerated the wound healing process by regulating inflammatory responses and recruiting suppressor cell types to the wound area.

Discussion

Dysbiosis of gut microbiota has been implicated in the etiology of a wide range of autoimmune/inflammatory diseases (41, 42). The ultimate goal of using bacteriotherapy to restore dysbiosis and prevent/treat pathological conditions holds great promise. However, given the considerable diversity in gut microbiota between individuals, what constitutes a "healthy" microbiome is not clear, making it difficult to define targets for microbial manipulation (43). Yet, gut microbiota hosts a multitude of immunomodulatory bacteria and/or bacteria-derived products waiting to be harnessed for therapeutic purposes (3, 44). In this study, we examined the immunomodulatory properties of MVs produced by the human symbiont *P. pentosaceus*. The rationale for using MVs was 3-fold: first, MVs play a major role in modulation of bacteria–host interactions (12). Second, MVs reproduce the immunoregulatory functions of the parent bacteria (7, 45). MVs can enter the circulation and distribute to various organs, eliciting systemic immunological and metabolic responses (46). Furthermore, a bacterial MV–based vaccine has already been approved by the European Medicines Agency since 2013, with no safety concerns after its widespread use in infants in the U.K. (47). Considering this safety record, we hypothesized that similar to a drug, bacterial MVs could be administered at a specified dose to modulate host responses reproducibly. As a proof of concept, we isolated MVs from a human lactic acid symbiont, *P. pentosaceus*. Consistent with previous reports, these Gram-positive MVs were enriched in cytoplasmic proteins, suggesting that cytoplasmic components were extruded through the weakened PGN layer by budding out (48–50). Importantly, our results demonstrate that *P. pentosaceus* MVs elicited immunosuppressive responses in fibrosis, vaccination, peritonitis, colitis, and wound healing models. Contrary to previous reports in which induction of Tregs was proposed as one of the mechanisms of action of *Bacteroides* and *Clostridium* species of MVs and/or bacteria (7, 9), *P. pentosaceus* MVs stimulated the generation MDSC- and M2 macrophage–like cells. This suggests that depending on the bacterial species of origin, MVs can elicit different groups of regulatory cells to control inflammation. Of note, *M. tuberculosis* MVs also elicit M-MDSC and G-MDSCs, but not Tregs, in vivo (51), supporting our observation.

Evidence suggests that TLR ligands enhance MDSC frequency and activity (52–55). Furthermore, the TLR2/1 agonist PAM3 preferentially supports the generation of immunosuppressive M2-like macrophages (39). Our data also suggest that *P. pentosaceus* MVs activate TLR2 signaling and that TLR2-mediated recognition most likely plays an important role in the MV-dependent polarization of immunosuppressive myeloid cells. Based on high expression levels of IL-10, Arg-1, and PD-L1 in MV-differentiated cells, it is likely that the immunoprotective effect of MV treatment in our fibrosis, peritonitis, colitis, and wound healing models could be through inhibition of inflammation through IL-10, arginase-1–mediated depletion of L-arginine and/or through the PD-L1/PD-1 pathway.

In conclusion, our results on *P. pentosaceus*–derived MVs have shown that these MVs have potent immunomodulatory effects. MVs' capacity to mobilize and/or activate suppressive/regulatory cell types open up the possibility of harnessing their potential in the treatment of inflammatory diseases.

Acknowledgments

We thank Dr. Fadime Kiran for providing the *P. pentosaceus* and *L. salivarius* commensal bacterial strains used in this study. We thank Dr. Ayse Selcen Oguz Erdogan for histological analysis of tissue samples and Dr. Ahmet Terzioglu and Dr. Kadri Ozer for assistance with excisional wound healing model.

Disclosures

The authors have no financial conflicts of interest.

References

1. Kamada, N., S.-U. Seo, G. Y. Chen, and G. Núñez. 2013. Role of the gut microbiota in immunity and inflammatory disease. *Nat. Rev. Immunol.* 13: 321–335.
2. Chen, F., and T. S. Stappenbeck. 2019. Microbiome control of innate reactivity. *Curr. Opin. Immunol.* 56: 107–113.
3. Skelly, A. N., Y. Sato, S. Kearney, and K. Honda. 2019. Mining the microbiota for microbial and metabolite-based immunotherapies. *Nat. Rev. Immunol.* 19: 305–323.
4. Ivanov, I. I., K. Atarashi, N. Manel, E. L. Brodie, T. Shima, U. Karaoz, D. Wei, K. C. Goldfarb, C. A. Santee, S. V. Lynch, et al. 2009. Induction of intestinal Th17 cells by segmented filamentous bacteria. *Cell* 139: 485–498.
5. Gaboriau-Routhiau, V., S. Rakotobe, E. Lécuyer, I. Mulder, A. Lan, C. Bridonneau, V. Rochet, A. Pisi, M. De Paepe, G. Brandi, et al. 2009. The key role of segmented filamentous bacteria in the coordinated maturation of gut helper T cell responses. *Immunity* 31: 677–689.
6. Tan, T. G., E. Sefik, N. Geva-Zatorsky, L. Kua, D. Naskar, F. Teng, L. Pasman, A. Ortiz-Lopez, R. Jupp, H.-J. J. Wu, et al. 2016. Identifying species of symbiont bacteria from the human gut that, alone, can induce intestinal Th17 cells in mice. *Proc. Natl. Acad. Sci. USA* 113: E8141–E8150.
7. Shen, Y., M. L. Giardino Torchia, G. W. Lawson, C. L. Karp, J. D. Ashwell, and S. K. Mazmanian. 2012. Outer membrane vesicles of a human commensal mediate immune regulation and disease protection. *Cell Host Microbe* 12: 509–520.
8. Atarashi, K., T. Tanoue, K. Oshima, W. Suda, Y. Nagano, H. Nishikawa, S. Fukuda, T. Saito, S. Narushima, K. Hase, et al. 2013. Treg induction by a rationally selected mixture of Clostridia strains from the human microbiota. *Nature* 500: 232–236.
9. Atarashi, K., T. Tanoue, T. Shima, A. Imaoka, T. Kuwahara, Y. Momose, G. Cheng, S. Yamasaki, T. Saito, Y. Ohba, et al. 2011. Induction of colonic regulatory T cells by indigenous *Clostridium* species. *Science* 331: 337–341.

10. Dehner, C., R. Fine, and M. A. Kriegel. 2019. The microbiome in systemic autoimmune disease: mechanistic insights from recent studies. *Curr. Opin. Rheumatol.* 31: 201–207.
11. Kaparakis-Liaskos, M., and R. L. Ferrero. 2015. Immune modulation by bacterial outer membrane vesicles. *Nat. Rev. Immunol.* 15: 375–387.
12. Yáñez-Mó, M., P. R. M. Siljander, Z. Andreu, A. B. Zavec, F. E. Borràs, E. I. Buzas, K. Buzas, E. Casal, F. Cappello, J. Carvalho, et al. 2015. Biological properties of extracellular vesicles and their physiological functions. *J. Extracell. Vesicles* 4: 27066.
13. Fábrega, M. J., L. Aguilera, R. Giménez, E. Varela, M. Alexandra Cañas, M. Antolín, J. Badía, and L. Baldomà. 2016. Activation of immune and defense responses in the intestinal mucosa by outer membrane vesicles of commensal and probiotic *Escherichia coli* strains. *Front. Microbiol.* 7: 705.
14. Birdsell, D. C., and E. H. Cota-Robles. 1967. Production and ultrastructure of lysozyme and ethylenediaminetetraacetate-lysozyme spheroplasts of *Escherichia coli*. *J. Bacteriol.* 93: 427–437.
15. Knox, K. W., M. Vesk, and E. Work. 1966. Relation between excreted lipopolysaccharide complexes and surface structures of a lysine-limited culture of *Escherichia coli*. *J. Bacteriol.* 92: 1206–1217.
16. Lee, E.-Y., D.-Y. Choi, D.-K. Kim, J.-W. Kim, J. O. Park, S. Kim, S.-H. Kim, D. M. Desiderio, Y.-K. Kim, K.-P. Kim, and Y. S. Gho. 2009. Gram-positive bacteria produce membrane vesicles: proteomics-based characterization of *Staphylococcus aureus*-derived membrane vesicles. *Proteomics* 9: 5425–5436.
17. Deatherage, B. L., and B. T. Cookson. 2012. Membrane vesicle release in bacteria, eukaryotes, and archaea: a conserved yet underappreciated aspect of microbial life. *Infect. Immun.* 80: 1948–1957.
18. Bitto, N. J., and M. Kaparakis-Liaskos. 2017. The therapeutic benefit of bacterial membrane vesicles. *Int. J. Mol. Sci.* 18: 1287.
19. Delbos, V., L. Lemée, J. Bénichou, G. Berthelot, A.-E. Deghmane, J.-P. Leroy, E. Houivet, E. Hong, M.-K. Taha, and F. Caron, B14 STOP Study Group. 2013. Impact of MenBvac, an outer membrane vesicle (OMV) vaccine, on the meningococcal carriage. *Vaccine* 31: 4416–4420.
20. Martinón-Torres, F., M. A. P. Safadi, A. C. Martinez, P. I. Marquez, J. C. T. Torres, L. Y. Weckx, E. D. Moreira, I. Mensi, M. Calabresi, and D. Toneatto. 2017. Reduced schedules of 4CMenB vaccine in infants and catch-up series in children: immunogenicity and safety results from a randomised open-label phase 3b trial. *Vaccine* 35: 3548–3557.
21. Pritsch, M., N. Ben-Khaled, M. Chaloupka, S. Kobold, N. Berens-Riha, A. Peter, G. Liegl, S. Schubert, M. Hoelscher, T. Löscher, and A. Wieser. 2016. Comparison of intranasal outer membrane vesicles with cholera toxin and injected MF59C.1 as adjuvants for malaria transmission blocking antigens AnAPN1 and Pfs48/45. *J. Immunol. Res.* 2016: 3576028.
22. Lee, T.-Y., C.-U. Kim, E.-H. Bae, S.-H. Seo, D. G. Jeong, S.-W. Yoon, K.-T. Chang, Y. S. Kim, S.-H. Kim, and D.-J. Kim. 2017. Outer membrane vesicles harboring modified lipid A moiety augment the efficacy of an influenza vaccine exhibiting reduced endotoxicity in a mouse model. *Vaccine* 35: 586–595.
23. Kang, C. S., M. Ban, E.-J. Choi, H.-G. Moon, J.-S. Jeon, D.-K. Kim, S.-K. Park, S. G. Jeon, T.-Y. Roh, S.-J. Myung, et al. 2013. Extracellular vesicles derived from gut microbiota, especially Akkermansia muciniphila, protect the progression of dextran sulfate sodium-induced colitis. *PLoS One* 8: e76520.
24. Spurbeck, R. R., and C. G. Arvidson. 2011. Lactobacilli at the front line of defense against vaginally acquired infections. *Future Microbiol.* 6: 567–582.
25. Rose, W. A. , II, C. L. McGowin, R. A. Spagnuolo, T. D. Eaves-Pyles, V. L. Popov, and R. B. Pyles. 2012. Commensal bacteria modulate innate immune responses of vaginal epithelial cell multilayer cultures. *PLoS One* 7: e32728.
26. Kanmani, P., and H. Kim. 2018. Protective effects of lactic acid bacteria against TLR4 induced inflammatory response in hepatoma HepG2 cells through modulation of toll-like receptor negative regulators of mitogen-activated protein kinase and NF-κB signaling. *Front. Immunol.* 9: 1537.
27. Bouladoux, N., J. A. Hall, J. R. Grainger, L. M. dos Santos, M. G. Kann, V. Nagarajan, D. Verthelyi, and Y. Belkaid. 2012. Regulatory role of suppressive motifs from commensal DNA. *Mucosal Immunol.* 5: 623–634.
28. Lv, L.-X., X.-J. Hu, G.-R. Qian, H. Zhang, H.-F. Lu, B.-W. Zheng, L. Jiang, and L.-J. Li. 2014. Administration of *Lactobacillus* salivarius LI01 or Pediococcus pentosaceus LI05 improves acute liver injury induced by D-galactosamine in rats. *Appl. Microbiol. Biotechnol.* 98: 5619–5632.
29. Zhao, X., F. Higashikawa, M. Noda, Y. Kawamura, Y. Matoba, T. Kumagai, and M. Sugiyama. 2012. The obesity and fatty liver are reduced by plant-derived Pediococcus pentosaceus LP28 in high fat diet-induced obese mice. *PLoS One* 7: e30696.
30. Shi, D., L. Lv, D. Fang, W. Wu, C. Hu, L. Xu, Y. Chen, J. Guo, X. Hu, A. Li, et al. 2017. Administration of Lactobacillus salivarius LI01 or Pediococcus pentosaceus LI05 prevents CCl_4-induced liver cirrhosis by protecting the intestinal barrier in rats. *Sci. Rep.* 7: 6927.
31. Xu, Q., S. Gu, Y. Chen, J. Quan, L. Lv, D. Chen, B. Zheng, L. Xu, and L. Li. 2018. Protective effect of *Pediococcus pentosaceus* LI05 against *Clostridium difficile* infection in a mouse model. *Front. Microbiol.* 9: 2396.
32. Klinman, D. M., and T. B. Nutman. 1994. ELISPOT assay to detect cytokine-secreting murine and human cells. *Curr. Protoc. Immunol.* 10: 6.19.1–6.19.8.
33. de Moura Estevão, L. R., P. Cassini-Vieira, A. G. B. Leite, A. A. V. de Carvalho Bulhões, L. da Silva Barcelos, and J. Evêncio-Neto. 2019. Morphological evaluation of wound healing events in the excisional wound healing model in rats. *Bio Protoc.* 9: e3285.
34. Bendtsen, J. D., L. Kiemer, A. Fausbøll, and S. Brunak. 2005. Non-classical protein secretion in bacteria. *BMC Microbiol.* 5: 58.
35. Tashiro, Y., S. Ichikawa, M. Shimizu, M. Toyofuku, N. Takaya, T. Nakajima-Kambe, H. Uchiyama, and N. Nomura. 2010. Variation of physiochemical properties and cell association activity of membrane vesicles with growth phase in *Pseudomonas aeruginosa*. *Appl. Environ. Microbiol.* 76: 3732–3739.
36. Dean, S. N., D. H. Leary, C. J. Sullivan, E. Oh, and S. A. Walper. 2019. Isolation and characterization of *Lactobacillus*-derived membrane vesicles. *Sci. Rep.* 9: 877.
37. Skabytska, Y., F. Wölbing, C. Günther, M. Köberle, S. Kaesler, K.-M. Chen, E. Guenova, D. Demircioglu, W. E. Kempf, T. Volz, et al. 2014. Cutaneous innate immune sensing of toll-like receptor 2-6 ligands suppresses T cell immunity by inducing myeloid-derived suppressor cells. *Immunity* 41: 762–775.
38. Wang, J., Y. Shirota, D. Bayik, H. Shirota, D. Tross, J. L. Gulley, L. V. Wood, J. A. Berzofsky, and D. M. Klinman. 2015. Effect of TLR agonists on the differentiation and function of human monocytic myeloid-derived suppressor cells. *J. Immunol.* 194: 4215–4221.
39. Bayik, D., D. Tross, L. A. Haile, D. Verthelyi, and D. M. Klinman. 2017. Regulation of the maturation of human monocytes into immunosuppressive macrophages. *Blood Adv.* 1: 2510–2519.
40. Horuluoglu, B., D. Bayik, N. Kayraklioglu, E. Goguet, M. J. Kaplan, and D. M. Klinman. 2019. PAM3 supports the generation of M2-like macrophages from lupus patient monocytes and improves disease outcome in murine lupus. *J. Autoimmun.* 99: 24–32.
41. Naik, S., N. Bouladoux, C. Wilhelm, M. J. Molloy, R. Salcedo, W. Kastenmuller, C. Deming, M. Quinones, L. Koo, S. Conlan, et al. 2012. Compartmentalized control of skin immunity by resident commensals. *Science* 337: 1115–1119.
42. Belkaid, Y., and T. W. Hand. 2014. Role of the microbiota in immunity and inflammation. *Cell* 157: 121–141.
43. Messer, J. S., E. R. Liechty, O. A. Vogel, and E. B. Chang. 2017. Evolutionary and ecological forces that shape the bacterial communities of the human gut. *Mucosal Immunol.* 10: 567–579.
44. Geva-Zatorsky, N., E. Sefik, L. Kua, L. Pasman, T. G. Tan, A. Ortiz-Lopez, T. B. Yanortsang, L. Yang, R. Jupp, D. Mathis, et al. 2017. Mining the human gut microbiota for immunomodulatory organisms. *Cell* 168: 928–943.e11.
45. Al-Nedawi, K., M. F. Mian, N. Hossain, K. Karimi, Y.-K. Mao, P. Forsythe, K. K. Min, A. M. Stanisz, W. A. Kunze, and J. Bienenstock. 2015. Gut commensal microvesicles reproduce parent bacterial signals to host immune and enteric nervous systems. *FASEB J.* 29: 684–695.
46. Yu, Y. J., X. H. Wang, and G.-C. Fan. 2018. Versatile effects of bacterium-released membrane vesicles on mammalian cells and infectious/inflammatory diseases. *Acta Pharmacol. Sin.* 39: 514–533.
47. Bryan, P., S. Seabroke, J. Wong, K. Donegan, E. Webb, C. Goldsmith, C. Vipond, and I. Feavers. 2018. Safety of multicomponent meningococcal group B vaccine (4CMenB) in routine infant immunisation in the UK: a prospective surveillance study. *Lancet Child Adolesc. Health* 2: 395–403.
48. Toyofuku, M., N. Nomura, and L. Eberl. 2019. Types and origins of bacterial membrane vesicles. *Nat. Rev. Microbiol.* 17: 13–24.
49. Brown, L., J. M. Wolf, R. Prados-Rosales, and A. Casadevall. 2015. Through the wall: extracellular vesicles in Gram-positive bacteria, mycobacteria and fungi. *Nat. Rev. Microbiol.* 13: 620–630.
50. Wang, X., C. D. Thompson, C. Weidenmaier, and J. C. Lee. 2018. Release of *Staphylococcus aureus* extracellular vesicles and their application as a vaccine platform. *Nat. Commun.* 9: 1379.
51. Prados-Rosales, R., A. Baena, L. R. Martinez, J. Luque-Garcia, R. Kalscheuer, U. Veeraraghavan, C. Camara, J. D. Nosanchuk, G. S. Besra, B. Chen, et al. 2011. Mycobacteria release active membrane vesicles that modulate immune responses in a TLR2-dependent manner in mice. *J. Clin. Invest.* 121: 1471–1483.
52. Maruyama, A., H. Shime, Y. Takeda, M. Azuma, M. Matsumoto, and T. Seya. 2015. Pam2 lipopeptides systemically increase myeloid-derived suppressor cells through TLR2 signaling. *Biochem. Biophys. Res. Commun.* 457: 445–450.
53. Delano, M. J., P. O. Scumpia, J. S. Weinstein, D. Coco, S. Nagaraj, K. M. Kelly-Scumpia, K. A. O'Malley, J. L. Wynn, S. Antonenko, S. Z. Al-Quran, et al. 2007. MyD88-dependent expansion of an immature GR-1(+)CD11b(+) population induces T cell suppression and Th2 polarization in sepsis. *J. Exp. Med.* 204: 1463–1474.
54. Bunt, S. K., V. K. Clements, E. M. Hanson, P. Sinha, and S. Ostrand-Rosenberg. 2009. Inflammation enhances myeloid-derived suppressor cell cross-talk by signaling through toll-like receptor 4. *J. Leukoc. Biol.* 85: 996–1004.
55. Rieber, N., A. Brand, A. Hector, U. Graepler-Mainka, M. Ost, I. Schäfer, I. Wecker, D. Neri, A. Wirth, L. Mays, et al. 2013. Flagellin induces myeloid-derived suppressor cells: implications for *Pseudomonas aeruginosa* infection in cystic fibrosis lung disease. *J. Immunol.* 190: 1276–1284.